Unexpected decline of the ocean carbon sink under record-high sea surface temperatures in 2023

Jens Müller
jensdaniel.mueller@usys.ethz.ch
ETH Zurich https://orcid.org/0000-0003-3137-0883
Nicolas Gruber
ETH Zürich https://orcid.org/0000-0002-2085-2310
Aline Schneuwly
ETH Zurich
Dorothee Bakker
University of East Anglia https://orcid.org/0000-0001-9234-5337
Marion Gehlen
Institut Pierre Simon Laplace https://orcid.org/0000-0002-9688-0692
Luke Gregor
ETH Zurich
Judith Hauck
Alfred Wegener Institute, Helmholtz Centre for Polar and Marine Research https://orcid.org/0000-0003-4723-9652
Peter Landschützer
Flanders Marine Institute (VLIZ) https://orcid.org/0000-0002-7398-3293
Galen McKinley
Columbia University https://orcid.org/0000-0002-4072-9221

Article

Keywords:

Posted Date: November 12th, 2024

DOI: https://doi.org/10.21203/rs.3.rs-5198321/v1

Additional Declarations: There is **NO** Competing Interest.

Unexpected decline of the ocean carbon sink under record-high sea surface temperatures in 2023

Jens Daniel Müller[1*], Nicolas Gruber[1], Aline Schneuwly[1], Dorothee C.E. Bakker[2], Marion Gehlen[3], Luke Gregor[1], Judith Hauck[4,5], Peter Landschützer[6], Galen A. McKinley[7]

[1]Environmental Physics, Institute of Biogeochemistry and Pollutant Dynamics, ETH Zurich, Zurich, Switzerland.

[2]Centre for Ocean and Atmospheric Sciences, School of Environmental Sciences, University of East Anglia, Norwich, UK.

[3]Laboratoire des Sciences du Climat et de l'Environnement, LSCE-IPSL, CEA-CNRS-UVSQ, Université Paris-Saclay, Gif-sur-Yvette, France.

[4]Alfred-Wegener-Institut, Helmholtz-Zentrum für Polar- und Meeresforschung, Bremerhaven, Germany.

[5]Universität Bremen, Bremen, Germany

[6]Flanders Marine Institute (VLIZ), Jacobsenstraat 1, 8400 Ostend, Belgium.

[7]Columbia University and Lamont-Doherty Earth Observatory, Palisades, NY, USA.

*Corresponding author. Email: jensdaniel.mueller@usys.ethz.ch

Abstract

In 2023, sea-surface temperatures (SST) reached record highs. Based on historical responses, this SST anomaly would suggest an increased oceanic CO_2 uptake (-0.11±0.03 PgC yr^{-1}). In contrast, our observation-based estimates reveal that the global non-polar ocean absorbed about 10% less carbon than expected (+0.16±0.28 PgC yr^{-1}). This weakening occurred despite reduced CO_2 outgassing in the tropics associated with El Niño. Hence, the decline in CO_2 uptake in 2023 materialised entirely in the extratropics, driven primarily by elevated SSTs in the Northern Hemisphere. Two ocean biogeochemical models demonstrate that in the subtropical North Atlantic the thermally-induced reduction in CO_2 uptake was strongly mitigated by the depletion of dissolved inorganic carbon in the surface mixed layer. Such negative feedbacks cause an overall muted response of the ocean carbon sink to the record high SSTs, but this resilience may not persist under long-term warming or more severe SST extremes.

Main

In 2023, sea surface temperatures (SST) across most of the ocean reached record highs[1–3]. Global warming is a main driver of this anomalous state of the surface ocean, but even when accounting for the linear trend in SST over the past 34 years, the annual mean anomaly of +0.21±0.02 °C was the largest ever observed between 50°S and 65°N (Fig. 1a). Apart from global warming, a strong El Niño was an important contributor to this unprecedented SST anomaly[1]. The spatial pattern of the SST anomalies represented in many parts the typical response to this phenomenon (Fig. 1b), but unusually high temperatures in the North Atlantic made 2023 distinct from previous years[4].

Here, we aim to establish how these extreme SSTs impacted the ocean's uptake of CO_2 from the atmosphere. This understanding is critical given that the ocean currently removes about a quarter of the annual anthropogenic CO_2 emissions from the atmosphere[5,6], but inevitable further global warming[7] and the increasing occurrence of anomalously high SSTs[8–10] might affect the functioning of this sink.

It is well established that warming reduces the solubility of CO_2 in seawater, favouring an increased outgassing of CO_2 to the atmosphere[11]. Under isochemical conditions, that is when the dissolved inorganic carbon (DIC) concentration and alkalinity (TA) remain constant, each 1°C rise in temperature increases the fugacity of CO_2 (fCO_2) by ~4%[12]. Thus, in the absence of any compensating mechanism, the 2023 SST anomaly of +0.2°C would have raised fCO_2 by 4 µatm, largely eliminating the mean sea-air fCO_2 gradient (ΔfCO_2) over the non-polar global ocean[13] and ceasing the uptake of CO_2 from the atmosphere.

However, non-thermal processes — such as changes in ocean circulation, mixing, and biogeochemical processes — can compensate for these thermal effects by modifying DIC and TA concentrations[14]. Thermal and non-thermal drivers are often in a delicate balance, which is well documented for the seasonal cycle of surface ocean fCO_2[12,15,16]. In some cases, non-thermal processes even overcompensate the direct temperature effect. This was observed during previous El Niño years, when the oceanic uptake of CO_2 became unusually strong (Fig. 1a) despite anomalously high global SSTs. This strengthening of the ocean carbon sink during El Niño resulted from the reduced outgassing of CO_2 in the eastern equatorial Pacific by roughly 0.1 - 0.2 PgC yr^{-1}, due to reduced upwelling of cold and CO_2-rich waters[17]. In contrast, the seasonal cycle of fCO_2 in the subtropics is thermally controlled, so that exceptionally warm SSTs are associated with an anomalous outgassing of CO_2[18]. Hence, the overall response of the ocean carbon sink to unusual warming depends sensitively on the regional distribution of the SST anomalies and the outcome of the "tug of war" between the thermal and non-thermal drivers of the surface ocean carbon cycle.

To quantify the impact of 2023's record high SSTs on the oceanic CO_2 uptake, we employ four observation-based fCO_2 products[19–22]. The fCO_2 products are machine-learning-based statistical models trained on in-situ fCO_2 observations from version 2023 of the Surface Ocean CO_2 Atlas (SOCAT) that provides observations through December 2022[23]. We mapped surface ocean fCO_2 through the end of 2023, using observed predictor fields for this year and assuming that the diagnosed relationships between fCO_2 and the predictors remain robust. This assumption was validated through prediction skill assessments based on truncated training data and comparisons to limited fCO_2 observations from 2023 (see SI)[23–26]. From the mapped fCO_2 fields, we computed the sea-to-air CO_2 flux (FCO_2) as the product of ΔfCO_2, the wind-dependent gas transfer velocity (k_w), and the solubility of CO_2 in seawater (K_0) (see Methods). Additionally, we employed hindcast simulations from two global ocean biogeochemical models (GOBM)[27,28], physically forced with reanalysis data[29], to explore how physical and biogeochemical anomalies in the ocean interior shape the surface anomalies.

We focus our study on low- and mid-latitudes between ~50°S and ~65°N, referred to as the global non-polar ocean. The Arctic and parts of the Southern Ocean are excluded due to remaining challenges in mapping interannual and seasonal flux anomalies in these regions, as highlighted by both previous studies[30,31] and our own analysis (Extended Data Figs. 3,4).

Results

Impact of record-high SSTs on the oceanic CO_2 uptake

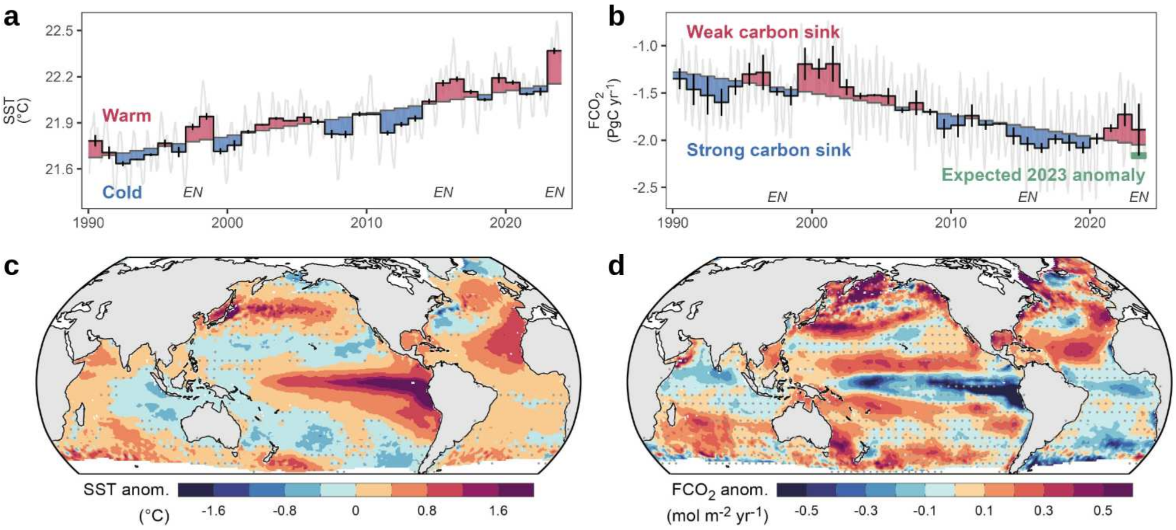

Fig. 1: Diagnosis of the record high sea surface temperatures (SST) in 2023 and their impact on sea-to-air CO_2 fluxes (FCO_2). (a) Timeseries of mean SST over the region between 50°S and 65°N based on the ensemble mean of four fCO_2 products (Table S1). Shown are annual (thick lines) and monthly mean (thin lines) values. Annual mean anomalies relative to the long-term trend are shaded in red and blue. Error bars indicate the spread of the annual anomalies across the four fCO_2 products. EN labels indicate strong El Niño years. (b) As (a), but for FCO_2. The green area in 2023 indicates the FCO_2 range expected from the linear relationship between FCO_2 and SST anomalies between 1990 and 2022 (Table S3). (c) Maps of the SST anomalies for 2023 relative to extrapolated long-term trend. Stippling indicates regions where the ensemble standard deviation is higher than the anomaly. (d) As (c), but for the FCO_2 anomalies.

The four observation-based fCO_2 products infer for 2023 an anomalous weakening of the ocean carbon sink by +0.16±0.28 PgC yr^{-1} integrated over our global non-polar analysis region (Fig. 1bd, Table 1). Note that we report sea-to-air CO_2 fluxes, that is, an ocean CO_2 uptake is negative, and an outgassing is positive. The 2023 flux anomaly corresponds to a roughly 10% reduction in CO_2 uptake. We computed this anomaly relative to a baseline that accounts for the linear trend from 1990 through 2022 (Fig. 1b, Methods), representing the increase in the uptake of CO_2 due to rising atmospheric CO_2 [6]. The decline of the ocean carbon uptake in 2023 is not unprecedented over the past 34 years, but it is unusual to occur in a year with record high SST (Fig. 2a). Based on the (largely El Niño-driven) relationship between annual mean anomalies in SST and ocean CO_2 uptake over the global non-polar ocean (Fig. 2a), one would have expected for 2023 an anomalously strong uptake of -0.12±0.03 PgC yr^{-1} (Fig. 1b,2a). Thus, something must have been different in 2023 compared to previous exceptionally warm years.

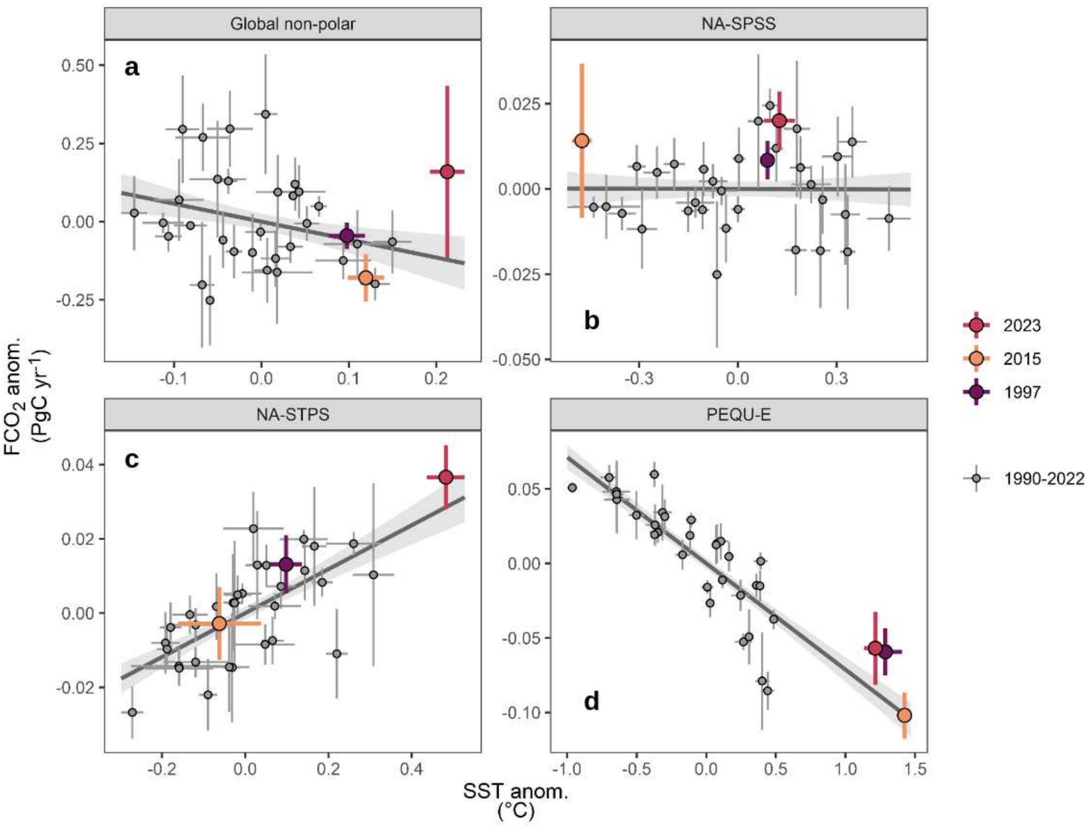

Fig. 2: Relationship between annual mean SST and sea-to-air CO_2 flux anomalies from 1990 to 2023 relative to the respective long-term trends. Anomalies are shown for (a) the global, non-polar ocean, (b) the North Atlantic subpolar seasonally stratified biome (NA-SPSS) (c) the North Atlantic subtropical permanently stratified biome (NA-STPS), and (d) the Pacific Equatorial Upwelling East biome (PEQU-E). Symbols and error bars represent the mean and standard deviation across the ensemble of four observation-based fCO_2 products, with the El Niño years 2023, 2015 and 1997 highlighted in warm colours. The grey lines and ribbons indicate linear regressions and 68% confidence intervals across all annual mean anomalies from 1990 to 2022. A biome map and correlation plots for other biomes are provided in the Extended Data Figs. 2 and 3, respectively.

The exceptional reduction of the ocean CO_2 uptake in 2023 was not caused by the eastern equatorial Pacific (PEQU-E). This biome actually experienced a reduced outgassing of CO_2 by -0.06±0.02 PgC yr^{-1}, i.e., an anomalous uptake. This CO_2 flux anomaly is very consistent with the expectation based on the SST anomaly in 2023 (Fig. 2d), and matches the response to previous El Niño events[17,32,33]. Slightly reinforced by reduced CO_2 outgassing from the tropical Atlantic and Indian Ocean (Fig. 1d), the flux anomalies integrated over the global tropics amounted to -0.07±0.05 PgC yr^{-1} (Table 1). This reduced outgassing from the tropics alone matches the expected uptake anomaly for the global ocean (Fig. 1a).

Hence, the decline of the CO_2 uptake must have occurred entirely in the extratropical ocean. Here, widespread positive SST anomalies, especially in the northern hemisphere (Fig. 1c), triggered an anomalous outgassing of CO_2 (Table 1).

Among the extratropical regions, the North Atlantic experienced the highest, most persistent and extensive SST anomalies in 2023. In particular the subtropical permanently stratified biome (NA-STPS) faced an unprecedented annual mean SST anomaly of +0.48±0.05 °C, which caused a substantial decline of the CO_2 uptake by +0.04±0.01 Pg C yr^{-1} (Table 1). This response fits the historic relationship between the CO_2 flux and SST anomalies very well (Fig. 2c), although the SST anomaly exceeds the previous record over the past 34 years by more than 50%. The two seasonally stratified biomes in the subtropical (NA-STSS) and subpolar (NA-SPSS) North Atlantic experienced similar CO_2 flux density anomalies as the NA-STPS, despite weaker annual mean SST anomalies (Table 1). However, the integrated CO_2 flux anomalies in the two seasonally stratified biomes are substantially lower than in

STPS, due to their smaller surface area. In total, the North Atlantic contributed a flux anomaly of +0.07±0.01 PgC yr^{-1} to the weakening of the ocean carbon sink in 2023.

In 2023, the CO_2 uptake weakened also in all biomes of the North Pacific (Table 1). The strongest anomalous outgassing occurred in the subtropical permanently stratified (NP-STPS) biome (+0.05±0.06 PgC yr^{-1}). The two smaller biomes (NP-STSS and NP-SPSS) contributed less to the weakening of the global ocean carbon sink, although the anomalies of their flux densities were about twice as strong as in the STPS biome (Fig. 1d, Table 1). Together, the North Pacific contributed +0.11±0.12 Pg C yr^{-1} to the total flux anomaly for the year 2023.

The subtropical permanently stratified biomes of the southern hemisphere reveal a more mixed picture with regard to the 2023 anomalies. Even though all three basins showed a positive SST anomaly, the CO_2 fluxes responded differently. While the STPS biomes in the Indian and Pacific also showed anomalous outgassing in 2023, the Atlantic STPS actually experienced a minor anomalous uptake. Considering also the STSS biome of the Southern Ocean, the extratropics of the southern hemisphere contributed in total +0.06±0.14 Pg C yr^{-1} to the global flux anomaly.

In the analysis above, we formally quantified the uncertainty of our estimates as the standard deviation across four observation-based fCO_2 products. For most parts of the tropics and the North Atlantic, we have high confidence in our estimates given that the fCO_2 products agree in sign and magnitude (Table 1, Extended Data Fig. 4). Due to the larger spread in the North Pacific and southern hemisphere biomes, we assign only medium confidence to our estimates in these regions. In particular, the fCO_2-Residual product suggests a substantially stronger weakening of the CO_2 sink in the North Pacific (Extended Data Figs. 1,4), reflecting the general tendency of this product to generate a strong interannual variability (Extended Data Fig. 1). The spread in the integrated flux anomalies from the North Pacific and southern hemisphere propagates to our estimates for the non-polar global ocean (Table 1, Extended Data Fig. 4), which range from a minor strengthening of the sink by -0.05 Pg yr^{-1} (CMEMS) to a strong weakening by almost +0.5 Pg yr^{-1} (fCO_2-Residual). As the fCO_2 products agree (mostly) in sign but not in magnitude, we assign a medium confidence to our flux anomaly estimates for the non-polar global ocean. However, when compared against the expectation of an anomalous strengthening of the sink (-0.12±0.03 PgC yr^{-1}) instead of the zero flux anomaly at the baseline (Fig. 1b), the consistency of our estimates is higher. Hence, we have high confidence in our conclusion that the ocean carbon sink in 2023 was indeed weaker than one would expect based on the SST anomaly.

Table 1: Annual mean CO_2 fluxes (FCO_2) and sea surface temperatures (SST) in 2023 together with the respective anomalies relative to a linear regression baseline. SST estimates are regional averages (°C), whereas FCO_2 estimates are given both as integrals (PgC yr^{-1}) and regional averages (mol m^{-2} yr^{-1}). All estimates represent the mean ± standard deviation over four observation-based fCO_2 products. Biomes abbreviations stand for: Subpolar seasonally stratified (SPSS), subtropical seasonally stratified (STSS), subtropical permanently stratified (STPS), the eastern and western equatorial Pacific (PEQU-E and PEQU-W), the tropical Atlantic and Indian Ocean (AEQU and Equ. Ind.), South Atlantic (SA), South Pacific (SP), and Southern Ocean (SO), according to the biome mach shown in the Extended Data Fig. 2. The anomaly estimates from this table are also presented in Extended Data Fig. 4.

		SST (°C)		FCO_2 (mol m^{-2} yr^{-1})		FCO_2 (Pg yr^{-1})	
Region	**Biome**	**Abs.**	**Anom.**	**Abs.**	**Anom.**	**Abs.**	**Anom.**
North Atl.	SPSS	+8.73±0.08	+0.13±0.05	-2.61±0.17	+0.18±0.08	-0.29±0.02	+0.02±0.01
	STSS	+19.02±0.03	+0.25±0.03	-2.19±0.25	+0.12±0.1	-0.16±0.02	+0.01±0.01
	STPS	+26.02±0.05	+0.48±0.05	-0.22±0.04	+0.14±0.03	-0.06±0.01	+0.04±0.01
	Total	**+20.63±0.02**	**+0.36±0.02**	**-1.12±0.08**	**+0.15±0.01**	**-0.51±0.03**	**+0.07±0.01**
North Pac.	SPSS	+8.91±0.1	+0.37±0.03	-1.09±0.28	+0.2±0.3	-0.18±0.05	+0.03±0.05
	STSS	+19.47±0.05	+0.43±0.05	-2.2±0.19	+0.22±0.11	-0.21±0.02	+0.02±0.01
	STPS	+26±0.03	0±0.03	-0.35±0.15	+0.1±0.13	-0.18±0.08	+0.05±0.06
	Total	**+21.5±0.01**	**+0.13±0.01**	**-0.74±0.17**	**+0.14±0.16**	**-0.58±0.14**	**+0.11±0.12**
NH extratropics		**+21.18±0.01**	**+0.21±0.01**	**-0.88±0.12**	**+0.14±0.1**	**-1.09±0.16**	**+0.17±0.12**
Tropics	PEQU-E	+27.45±0.08	+1.21±0.08	+1.67±0.16	-0.31±0.13	+0.3±0.03	-0.06±0.02
	PEQU-W	+29.57±0.07	+0.04±0.03	+0.23±0.06	+0.05±0.03	+0.04±0.01	+0.01±0.01
	AEQU	+27.57±0.03	+0.23±0.08	+0.19±0.18	-0.11±0.13	+0.02±0.02	-0.01±0.01
	Equ. Ind.	+28.32±0.03	+0.01±0.06	+0.31±0.1	-0.02±0.08	+0.1±0.04	-0.01±0.03
	Total	**+28.28±0.05**	**+0.33±0.05**	**+0.59±0.06**	**-0.09±0.06**	**+0.46±0.05**	**-0.07±0.05**
SH extratropics	SA-STPS	+22.94±0.03	+0.11±0.04	-0.21±0.05	-0.06±0.06	-0.05±0.01	-0.01±0.01
	SP-STPS	+22.29±0.02	+0.11±0.03	-0.29±0.19	+0.06±0.14	-0.19±0.13	+0.04±0.09
	South. Ind.	+22.35±0.03	+0.11±0.09	-1.15±0.05	+0.13±0.11	-0.24±0.01	+0.03±0.02
	SO-STSS	+13.2±0.08	+0.28±0.07	-2.24±0.27	+0.02±0.14	-0.79±0.1	+0.01±0.05
	Total	**+20.21±0.02**	**+0.15±0.04**	**-0.87±0.15**	**+0.04±0.1**	**-1.26±0.23**	**+0.06±0.14**
Global non-polar		**+22.36±0.02**	**+0.21±0.02**	**-0.55±0.11**	**+0.05±0.08**	**-1.89±0.38**	**+0.16±0.28**
Polar	SO-SPSS	+3.88±0.11	+0.13±0.04	-0.6±0.59	-0.17±0.38	-0.22±0.22	-0.06±0.14
	SO-ICE	-0.95±0.07	+0.09±0.04	-0.57±0.29	-0.05±0.2	-0.13±0.05	-0.01±0.04
	Arctic	-0.14±0.41	-0.07±0.09	-1.5±0.58	+0.29±0.12	-0.14±0.02	+0.03±0.02
Global		**+18.74±0.01**	**+0.19±0.01**	**-0.58±0.15**	**+0.03±0.1**	**-2.38±0.65**	**+0.12±0.43**

Driver attribution and seasonality of CO_2 flux anomalies

The annual mean CO_2 flux anomaly over the non-polar global ocean in 2023 was primarily (>95%) driven by anomalies in ΔfCO_2 (Fig. 3a, S5). The ΔfCO_2 anomaly triggered positive CO_2 flux anomalies (i.e. a weaker sink) in all regions that experienced a positive SST anomaly, except in the eastern equatorial Pacific (Figs. 1a,3a). Anomalies in wind speed further modulated the annual mean CO_2 flux at regional scales (Fig. 3b), for example the central equatorial Pacific or the North Pacific off Japan, but had a small net impact on globally integrated fluxes (Extended Data Fig. 5). The modulation of ΔfCO_2-driven flux anomalies through wind anomalies (i.e. the cross term $\Delta fCO_2 \times k_w K_0$) is negligible on regional scales, as well as for the globally integrated flux anomalies (Fig. 3c, Extended Data Fig. 5), and will not be discussed further.

To quantify the causes for the 2023 anomalies in ΔfCO_2, we further decomposed the main contributor, which is the oceanic fCO_2 anomaly, into a thermal and a non-thermal component (see Methods). The regions with the strongest SST anomalies reveal by definition the largest thermal component of the fCO

$_2$ anomaly, i.e., the eastern equatorial Pacific, subpolar North Pacific, and subtropical North Atlantic (Fig. 3d). The same regions experienced also the strongest non-thermal component of the fCO_2 anomaly (Fig. 3e). Hence, the resulting total fCO_2 anomaly remained comparably small at regional scales (Fig. 3f), and were slightly positive (+0.05±0.1 µatm) when averaged over the global non-polar ocean (Extended Data Fig. 6).

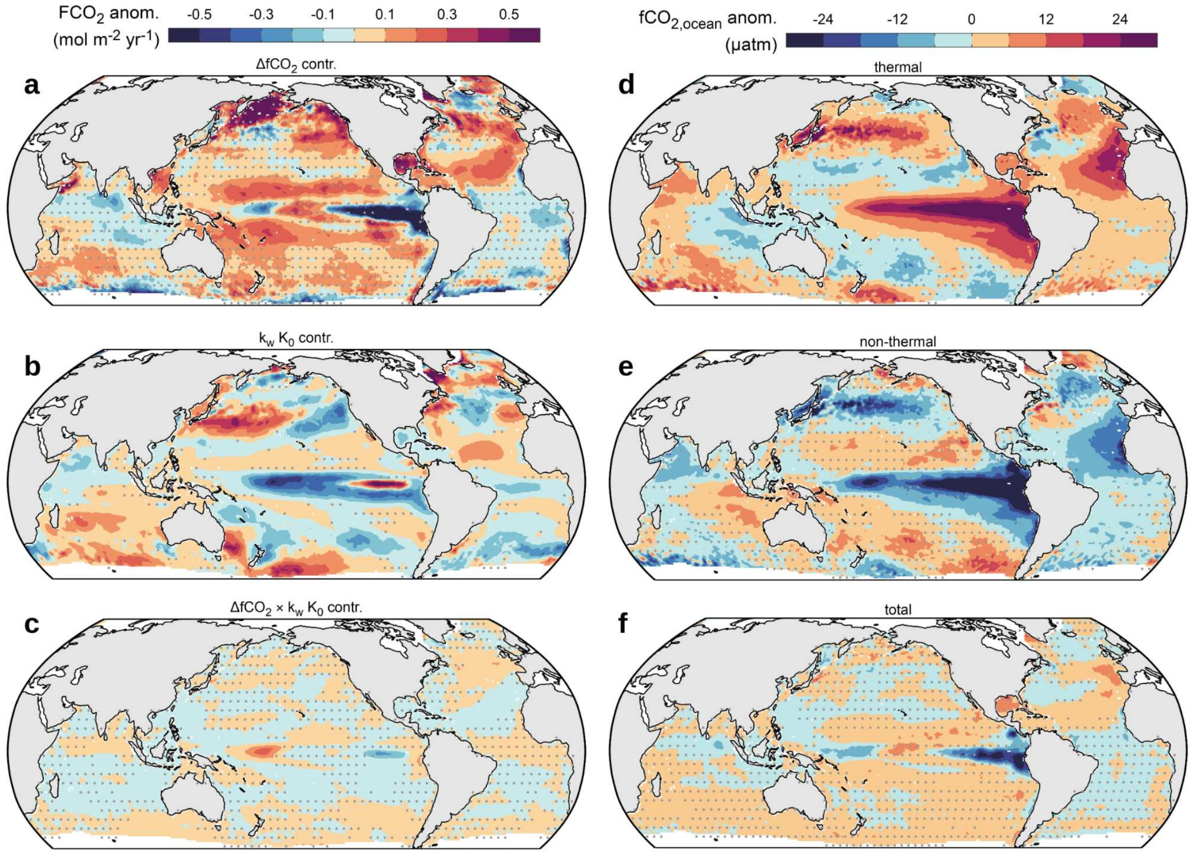

Fig. 3: Attribution of 2023 annual mean flux anomalies and fCO_2 decomposition. (a-c) Attribution of flux anomalies to their primary drivers, that is, (a) the CO_2 fugacity gradient between ocean and atmosphere (ΔfCO_2), (b) the product of the gas transfer velocity and the solubility of CO_2 ($k_w K_0$), which is primarily controlled by wind speed, as well as (c) the cross product of both drivers ($\Delta fCO_2 \times k_w K_0$). (d-f) Decomposition of (f) the total fCO_2 anomalies into the (d) thermal and (e) non-thermal components. Stippling indicates regions where the ensemble standard deviation is higher than the absolute ensemble mean.

To dive further into the attribution of the 2023 CO_2 flux anomalies, we contrast their seasonal evolution and drivers for three biomes. For this purpose, we corroborate the observation-based surface anomalies with vertically resolved simulations from two GOBMs. Our GOBMs simulate a similar seasonal evolution of the SST and CO_2 flux anomalies in 2023 compared to the observation-based estimates (Fig. 4, Extended Data Fig. 7) and are therefore considered reliable tools to interpret the underlying physical and biogeochemical processes.

The seasonal evolution of SST anomalies in the eastern equatorial Pacific (PEQU-E) resembles that of previous El Niño events. A positive SST anomaly of around 2°C established gradually over the first half of 2023 and remained rather stable thereafter (Fig. 4a). This SST evolution was mirrored in a reduction of the outgassing of CO_2 (i.e., a growing CO_2 sink) by up to 0.5 mol m^{-2} yr^{-1}. The reduced outgassing was primarily a consequence of negative ΔfCO_2 anomalies, but reinforced by anomalously low wind speeds.

The negative ΔfCO_2 anomalies in PEQU-E resulted from reduced upwelling of remineralized DIC. To quantify this well-known non-thermal driver, we subtract the salinity-normalised alkalinity (sTA) anomaly from the anomaly in salinity-normalised dissolved inorganic carbon (sDIC), and convert the anomalous decline of sDIC-sTA (~- 20 µmol kg^{-1}; Fig. 4b) into an equivalent fCO_2 reduction of roughly 40 µatm (see Methods). This DIC-driven fCO_2 reduction is already muted by the reduced outgassing of CO_2 that occurred over the course of 2023, but it still remains substantially stronger than the temperature-driven increase of fCO_2 by ~30 µatm at the end of the year. Hence, the non-thermal component clearly won the “tug of war” in PEQU-E.

In the subtropical permanently stratified biome of the North Atlantic (NA-STPS), the monthly SST anomalies peaked in summer at around +1°C and remained well above the range of past anomalies for the remainder of 2023. In contrast to PEQU-E, the resulting CO_2 flux anomaly in NA-STPS was positive, that is, the CO_2 uptake in winter became weaker and the outgassing in summer became stronger. This anomalous outgassing was primarily driven by thermally-driven ΔfCO_2 anomalies (Fig. 4a, Extended Data Figs. 5,6) and slightly enhanced by weak winds that further reduced the CO_2 uptake from January to April (Extended Data Fig. 7). The mixed layer depth simulated by the GOBMs was anomalously shallow in 2023, suggesting increased stratification and reduced mixing of remineralized DIC into the surface layer (Extended Data Fig. 8). However, the simulated sDIC-sTA anomalies of -3 µmol kg^{-1} in NA-STPS were much weaker than in PEQU-E. This sDIC-sTA anomaly was established primarily in summer, when the surface CO_2 flux anomalies were also strongest (Fig. 4a). Integrated over the summertime mixed layer depth of ~50m, the sDIC-sTA inventory decreased by roughly 0.15 mol m^{-2} over the course of 2023 (Fig. 4b), which is almost identical to the cumulative CO_2 flux anomaly. This suggests that the surface CO_2 flux anomaly was the primary driver of the inventory anomaly in the surface mixed layer. Hence, the reduced mixing of DIC into the surface layer — due the increased stratification — was either negligibly small or nearly balanced by reduced primary production of organic matter (Extended Data Fig. 8). Overall, the thermal driver won the "tug of war” and determined the CO_2 flux anomalies during the onset of the SST anomaly in NA-STPS.

In the subpolar seasonally stratified biome of the North Atlantic (NA-SPSS), the monthly peak SST anomalies were about as high as in NA-STPS, but more confined to the summer months and less exceptional when compared to the variability in previous decades (Fig. 4a). Likewise, the CO_2 flux anomalies were less exceptional. In contrast to NA-STPS, wind anomalies played a major role in regulating the 2023 CO_2 fluxes in NA-SPSS (Extended Data Figs. 5,7). Strong winds until May favoured the natural CO_2 sink, whereas weak winds throughout the rest of 2023 reduced the natural sink and thereby reinforced the anomalous outgassing triggered by positive ΔfCO_2 anomalies. The interpretation of the GOBM simulations in the NA-SPSS biome is rather complex. The simulated summertime temperature increase was confined to a very shallow surface layer (10-20m) and triggered a higher ΔfCO_2 anomaly than in the fCO_2 products, due to a weaker non-thermal fCO_2 anomaly in the GOBMs (Extended Data Fig. 7). However, GOBMs are known to underestimate the non-thermal fCO_2 component in the seasonal cycle[16] in the NA-SPSS biome, which also hampers the interpretation of biogeochemical drivers of the 2023 anomalies.

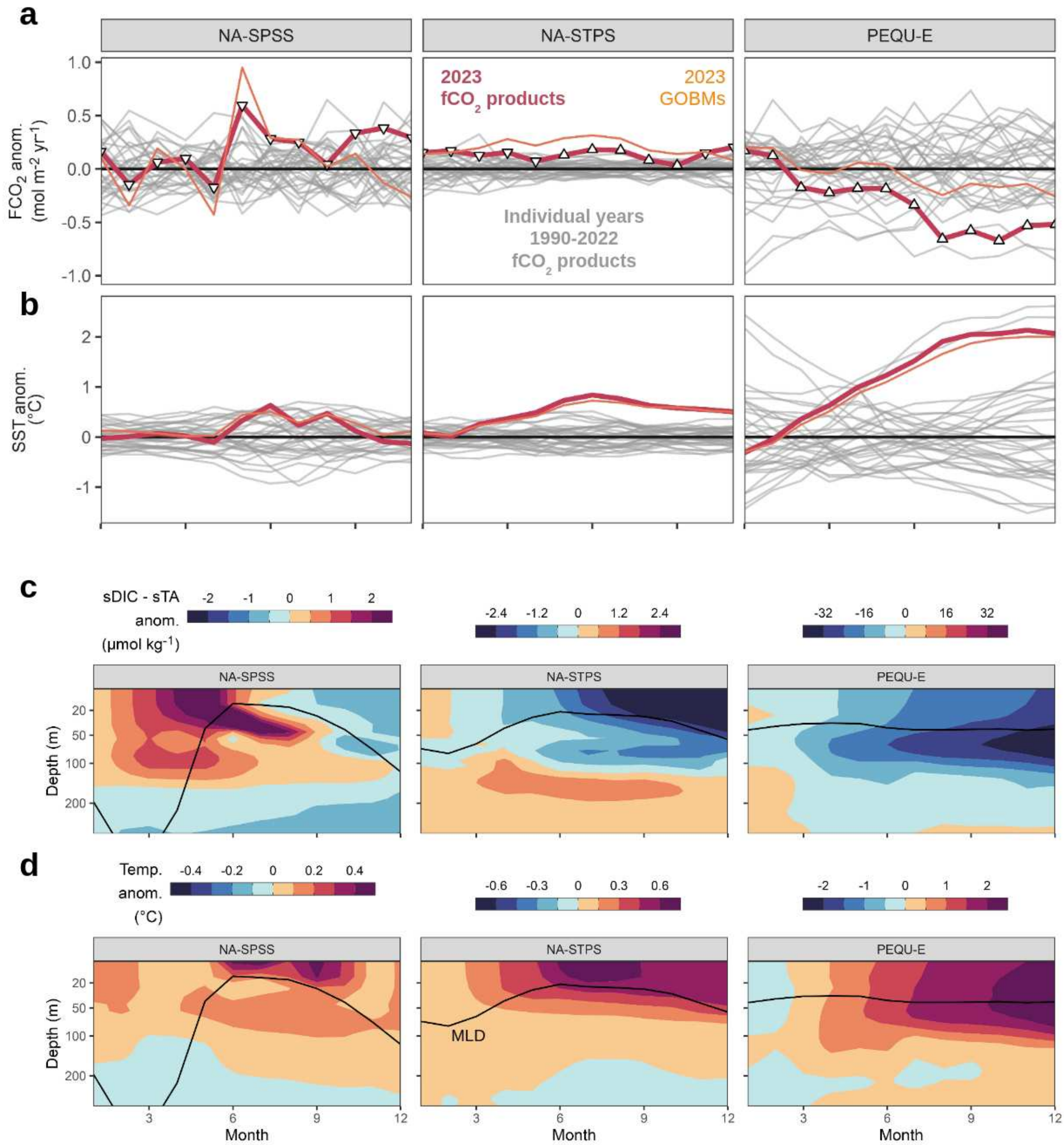

Fig. 4: Seasonal anomaly evolution for three key biomes. (a,b) Monthly mean surface anomalies of (a) the CO_2 flux density, with triangles indicating the direction of the prevailing absolute CO_2 flux into (downwards) or out of (upwards) the ocean, and (b) SST. Red and grey lines represent the fCO_2 product ensemble mean, whereas the orange line represents the GOBM ensemble mean for 2023. (c,d) Vertical mean monthly anomalies of (c) salinity-normalised DIC (sDIC) anomalies, adjusted for the anomaly in salinity-normalised TA (sTA) to capture the sDIC anomaly that is directly linked to fCO2 anomalies, and (d) temperature. The sDIC anomalies are presented as changes since January 2023, to remove legacy anomalies from 2022 and achieve direct comparability to the instantaneous surface flux anomalies. Black lines indicate the mean mixed layer depth (MLD). All vertical anomalies represent the mean of the two GOBMs.

Discussion

In this study, we demonstrated that widespread and record-high SST led to a reduction in the ocean's carbon sink in 2023. The anticipated anomalous CO_2 uptake in the tropics was outweighed by an increase in CO_2 outgassing from the non-polar extratropics (Fig. 5b). Among these regions, the anomalous CO_2 outgassing in the subtropical North Atlantic, driven by unusually strong and persistent SST anomalies (Fig. 5a), stood out as a strong and robust feature.

Interestingly, the depletion of DIC in NA-STPS by the end of 2023, reflected by the sDIC-sTA anomaly of -3 µmol kg^{-1} (Fig. 4b), had an effect on surface ocean fCO_2 (~6 µatm) that was similar in magnitude but opposite in direction compared to that of the SST anomaly (+0.5°C). This suggests that the DIC-depletion fully compensated the thermal driver by the end of the year. The resulting decline of the anomalous outgassing towards winter is indeed evident in our GOBM simulations, but less so in the observation-based fCO_2 products (Fig. 4a), suggesting that the DIC-depletion feedback may not be well captured by the underlying statistical models. If the DIC-depletion remained stable during the first half of 2024, the anomalous outgassing in NA-STPS may have ceased, despite the continued elevated SSTs. However, mixing during wintertime 2023/24 might have replenished the surface DIC pool. Hence, we expect a neutral to to reduced sink strength in NA-STPS in the first half of 2024.

In contrast to the near-balance of the thermal and non-thermal drivers in NA-STPS, the non-thermal DIC anomaly remained dominant in PEQU-E. By the end of 2023, the integrated anomaly of sDIC-sTA over the top 100 m had reached -2 mol m^{-2}, which far exceeded the CO_2 flux anomaly of about -0.1 mol m^{-2} that occurred cumulatively over the course of the year (Fig. 4). Hence, the remaining negative DIC anomaly could potentially drive further reduced outgassing, provided that these water masses stay in contact with the atmosphere. However, as SST anomalies in PEQU-E decreased during the first half of 2024, CO_2 outgassing in this biome most likely returned to normal levels. Hence, we expect a rather neutral sink strength in PEQU-E in the first half of 2023. If indeed the reduced outgassing in the tropics fades out, while the extratropics remain anomalously warm, the global ocean carbon sink might have continued to be weak in a weak state in early 2024. Whether these projected CO_2 flux anomalies indeed materialise in 2024 remains to be confirmed through fCO_2 observations.

The limitation of thermally-induced CO_2 outgassing by DIC-depletion – that we observed for the warming event in 2023 – is also crucial when considering the ocean carbon sink's long-term response to global warming. Between 2000 and 2019, warming weakened the oceanic uptake of CO_2[34], but the impact was much weaker than one would expect from the decreased solubility alone (i.e. the thermal driver). This is because the temperature-induced outgassing of CO_2 and the reduced upwelling of DIC (both non-thermal drivers) caused a negative feedback that compensated the initial perturbation. While these negative feedbacks have now been demonstrated for historic warming SST extremes and historic trends in the ocean carbon sink, it remains unclear if these stabilising mechanisms of the ocean carbon sink remain effective under extreme SST events in the future, which are expected to become more frequent, intense, and longer lasting[8], or under progressing global warming. Deviations from the negative feedbacks observed in the past could for example occur if longer lasting SST extremes cause stronger limitations of the CO_2 outgassing due to DIC-depletion, or if the efficiency of the biological carbon pump becomes more strongly affected. To keep track of potential surprises in the ocean carbon sink, the continued, revived, and extended observation of the ocean with high quality fCO_2 measurements remains indispensable, and it needs to be accompanied with an improved understanding of the fCO_2 mapping skill at seasonal to interannual time scales and across ocean biomes [30,31].

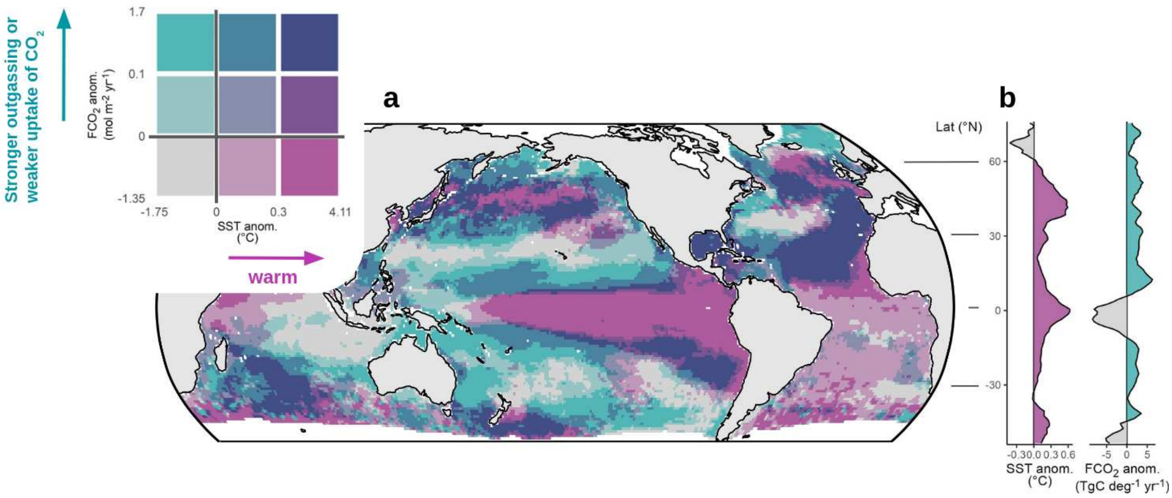

Fig. 5: (a) Bivariate map of 2023 annual mean anomalies in the CO_2 flux (FCO_2) and corresponding SST anomalies. (b) Annual mean fCO_2 anomalies (grey) and their decomposition into the thermal (red) and non-thermal (blue) component, for the eastern equatorial Pacific (PEQU-E) and subtropical permanently stratified biome of the North Atlantic (NA-STPS). All estimates are based on the ensemble mean of four fCO_2 products.

Methods

Data base

This study relies on four fCO_2 products and two global ocean biogeochemical models, for which technical details are provided in the Extended Data Tables 1 and 2, respectively. These data sources constitute a subset of those used in the Global Carbon Budget[5] and the second iteration of the REgional Carbon Cycle Assessment and Processes project (RECCAP2)[35,36]. The observation-based sea surface temperature fields used as predictor variables in the fCO_2 products are also used for our analysis of SST trends and anomalies. The GOBMs simulations used here are equivalent to those considered as "simulation A" in RECCAP2, that is, they are forced with (i) reanalysis data to represent the observed climate variability over the hindcast period and (ii) historic atmospheric CO_2 observations to represent anthropogenic emissions.

Anomaly determination against moving baseline

All anomalies determined in this study are expressed relative to a moving baseline, in order to remove the long-term trends that are driven by the growth in atmospheric CO_2 or global warming. The baseline estimate for any particular year (mostly 2023) was determined from a linear regression model that was fitted to the historic observations from 1990 through 2022, and then predicted for the year of interest. The underlying data are either annual or monthly mean values. The data for 2023 were excluded from the regression to achieve a baseline estimate that is unbiased from the actual anomaly in 2023. Linear regression models were applied to determine the baseline for any variable of interest, except for the atmospheric and surface ocean fCO_2, for which a quadratic fit was used to better approximate the actual growth rate. Finally, anomalies are calculated by subtracting the predicted baseline value from the observed or estimated value.

Expected FCO_2 anomaly in 2023

To determine the expected FCO_2 anomaly in 2023 for the global non-polar ocean, we fitted linear regression models of the integrated annual mean FCO_2 anomaly as a function of the annual mean SST anomaly to the hindcast estimates from 1990 through 2022 of our four fCO_2 products. The intercepts (in $PgC\ yr^{-1}$) and the slopes (in $PgC\ yr^{-1}\ °C^{-1}$) of these four regression models are: -1.3×10^{-14} and -0.61 (CMEMS), 1.9×10^{-15} and -0.74 (fCO_2-Residual), -4.6×10^{-15} and -0.39 (OceanSODAv2), and 1.8×10^{-16} and -0.43 (SOM-FFN).

Based on these regression models, the expected FCO_2 anomaly in 2023 was calculated for each fCO_2 product from the SST anomaly in 2023. The 2023 SST anomalies (in °C) and the derived expected FCO_2 anomalies (in $PgC\ yr^{-1}$) are: 0.19 and -0.12 (CMEMS), 0.2 and -0.15 (fCO_2-Residual), 0.22 and -0.09 (OceanSODAv2), and 0.23 and -0.1 (SOM-FFN). The mean and standard deviation of this expected FCO_2 anomaly is $-0.11 \pm 0.03\ PgC\ yr^{-1}$ (Fig. 1b).

Computation and attribution of flux anomalies

The CO_2 flux (FCO_2) across the air-sea interface is determined as the product of the fugacity difference between ocean and atmosphere (ΔfCO_2), the gas transfer velocity (k_w), and the solubility of CO_2 in seawater (K_0) and is scaled with the fractional ice coverage (f_{ice}) according to:

$$FCO_2 = \Delta fCO_2 \times (k_w K_0) \times (1 - f_{ice}) \quad (1)$$

The product $k_w K_0$ is largely temperature independent, because the temperature dependence in k_w and K_0 largely cancel out. Hence, $k_w K_0$ depends primarily on the prevailing wind speed. Applying a first order Taylor decomposition, one can attribute flux anomalies to their drivers as:

$$'FCO_2 = {‘}\Delta fCO_2 \times (k_w K_0)_{baseline} + \Delta fCO_{2,baseline} \times (k_w K_0) + '\Delta fCO_2 \times '(k_w K_0) \qquad (2)$$

, where prime (‘) symbols and the index “baseline” denote anomalies and detrended baseline estimates, respectively. The modulation by the fractional ice coverage is neglected in the attribution, as our study focuses on the ice-free ocean. We compute the flux anomaly contributions initially on the original grid of our estimates (1 monthly, 1°x1°) and then average the components in space and time (e.g. to compute biome annual means).

Thermal and non-thermal decomposition of fCO_2 anomalies

To assess the mechanistic drivers causing the 2023 anomalies in ΔfCO_2, we decomposed the main contributor to this anomaly, which is the surface ocean fCO_2 anomaly, into a thermal and a non-thermal component based on the sea surface temperature anomalies. We perform this decomposition initially on the original grid of our estimates (1 monthly, 1°x1°) and then average the components in space and time (e.g. to compute biome annual means).

Specifically, we determine in a first step the thermally-driven fCO_2 anomaly ($'fCO_{2,thermal}$) according to equation (3):

$$'fCO_{2,thermal} = fCO_{2,baseline} \times \exp(\gamma_T \times 'SST) - fCO_{2,baseline} \qquad (3)$$

, where $fCO_{2,baseline}$ is the monthly baseline value of fCO_2, γ_T is the temperature sensitivity of fCO_2 (0.0423 K^{-1})[12], and $'SST$ is the monthly anomaly in sea surface temperature. Note that the $fCO_{2,baseline}$ inherits a seasonal cycle and is expressed in absolute values that are similar to the observed fCO_2 values. In contrast, ‘SST represents only the deviation of the observed SST from the expected baseline value, i.e. it is a numerically small value of positive or negative sign and does not follow a classical seasonal cycle. As a consequence, the variable $'fCO_{2,thermal}$ computed according to equation (3) is also a numerically small value of positive or negative sign and does not follow a typical seasonal pattern. In this regard, our thermal anomaly component $'fCO_{2,thermal}$ differs from the widely used thermal component of fCO_2 that is defined as $fCO_{2,thermal} = fCO_{2,mean} \times \exp(\gamma_T \times (SST_{obs} - SST_{mean}))$. In this classical decomposition of absolute fCO_2 values (instead of anomalies), $SST - SST_{mean}$ and hence also $fCO_{2,thermal}$ follow a classical seasonal cycle, and the value of $fCO_{2,thermal}$ has the same order of magnitude as fCO_2 itself. $fCO_{2,thermal}$ can be considered as the seasonal cycle of fCO_2 driven solely by the seasonal cycle in SST.

Based on the anomaly components $'fCO_{2,thermal}$ and $'fCO_2$, we determine the non-thermally driven fCO_2 a nomaly ($'fCO_{2,non\text{-}thermal}$) as:

$$'fCO_{2,non\text{-}thermal} = 'fCO_2 - 'fCO_{2,thermal} \qquad (4)$$

While our definition of $'fCO_{2,non\text{-}thermal}$ according to equation (4) resembles the definition of the fCO_2 residual in previous works[19,37], it differs in that it does not inherit a classical seasonal cycle. Likewise, our anomaly component $'fCO_{2,non\text{-}thermal}$ differs from the widely used[15,38] non-thermal component of fCO_2 that is defined as $fCO_{2,non\text{-}thermal} = fCO_{2,obs} \times \exp(\gamma_T \times (SST_{mean} - SST_{obs}))$ and describes the fCO_2 seasonality that would occur if SST remained at the annual mean, but all other processes followed their natural seasonal cycle.

Conversion from DIC to fCO_2 anomalies

To convert DIC anomalies into fCO_2 anomalies, it is important to consider alkalinity (TA) anomalies that occur simultaneously, because the fraction of the DIC anomaly that is caused by the TA anomaly has no effect on fCO_2. The conversion can formally be derived by considering the sensitivity of fCO_2 to changes in either DIC or TA[14,39]:

$$\gamma_{DIC} = (\Delta fCO_{2,DIC} / fCO_2) / (\Delta DIC / DIC) \tag{5}$$

and

$$\gamma_{TA} = (\Delta fCO_{2,TA} / fCO_2) / (\Delta TA / TA) \tag{6}$$

Given that the total change in fCO_2 is the sum of the change driven by TA and DIC:

$$\Delta fCO_2 = \Delta fCO_{2,DIC} + \Delta fCO_{2,TA} \tag{7}$$

and assuming that to first order $\gamma_{DIC} \approx -\gamma_{TA}$ and DIC ≈ TA, one can insert the two sensitivities (5 and 6) in equation (7) and derive the expression:

$$\Delta fCO_2 = \gamma_{DIC} (fCO_2 / DIC) (\Delta DIC - \Delta TA) \tag{8}$$

One can interpret the term ΔDIC - ΔTA as the effective change in DIC that is not compensated for by a change in TA. Intuitively, a positive DIC anomaly that is not fully balanced by a TA anomaly would lead to a positive fCO_2 anomaly.

Interestingly, one can further introduce the approximation that the carbonate ion concentration $[CO_3^{2-}] \approx TA - DIC$. Hence, the changes in fCO_2 can also be expressed as:

$$\Delta fCO_2 = - \gamma_{DIC} (fCO_2 / DIC) \; \Delta[CO_3^{2-}] \tag{9}$$

This equation can be interpreted such that a positive anomaly in carbonate ion concentration is equivalent to a negative anomaly in fCO_2. Hence, our Fig. 4c could be redrawn with an inverted colour scale and showing $[CO_3^{2-}]$ instead of DIC -TA.

In this study, we used the salinity-normalised anomalies in DIC and TA for ΔDIC and ΔTA, respectively. We approximated the absolute values of DIC, fCO_2, and γ_{DIC} as 2000 µmol kg^{-1}, 420 µatm, and 10. It should be noted that this conversion only serves as a first-order approximation of the relationship between fCO_2 and DIC anomalies on biome scales.

Data availability

The surface ocean fCO_2 observations that were used for the training and validation of the fCO_2 products are publicly available under:

SOCATv2023: https://doi.org/10.25921/r7xa-bt92

SOCATv2024: https://doi.org/10.25921/9wpn-th28

For two stations, 2023 observations were sourced from SOCATv2024 and analysed in detail. The direct access to these data is possible through the following DOIs:

TAO170W: 10.3334/cdiac/otg.tsm_tao170w_0n

BATS: 10.25921/r7vk-e838

The fCO_2 products and GOBM simulations analysed in this study will be made available through Zenode and receive a doi upon acceptance of this article for publication.

Code availability

All code required to perform the analysis and prepare figures presented in this study is available under:

https://github.com/jens-daniel-mueller/heatwave_co2_flux_2023

Upon acceptance of this article for publication, the latest version of the code will be made available through Zenodo and receive a doi.

References

1. Huang, B. *et al.* Record High Sea Surface Temperatures in 2023. *Geophys. Res. Lett.* **51**, e2024GL108369 (2024).
2. Samset, B. H., Lund, M. T., Fuglestvedt, J. S. & Wilcox, L. J. 2023 temperatures reflect steady global warming and internal sea surface temperature variability. *Commun. Earth Environ.* **5**, 1–8 (2024).
3. Raghuraman, S. P. *et al.* The 2023 global warming spike was driven by El Niño/Southern Oscillation. *EGUsphere* 1–12 (2024) doi:10.5194/egusphere-2024-1937.
4. Kuhlbrodt, T., Swaminathan, R., Ceppi, P. & Wilder, T. A Glimpse into the Future: The 2023 Ocean Temperature and Sea Ice Extremes in the Context of Longer-Term Climate Change. *Bull. Am. Meteorol. Soc.* **105**, E474–E485 (2024).
5. Friedlingstein, P. *et al.* Global Carbon Budget 2023. *Earth Syst. Sci. Data* **15**, 5301–5369 (2023).
6. Gruber, N. *et al.* Trends and variability in the ocean carbon sink. *Nat. Rev. Earth Environ.* 1–16 (2023) doi:10.1038/s43017-022-00381-x.
7. IPCC. Climate Change 2021: The Physical Science Basis. Contribution of Working Group I to the Sixth Assessment Report of the Intergovernmental Panel on Climate Change. vol. In Press (2021).
8. Frölicher, T. L., Fischer, E. M. & Gruber, N. Marine heatwaves under global warming. *Nature* **560**, 360–364 (2018).
9. Jo, A. R., Lee, J.-Y., Sharma, S. & Lee, S.-S. Season-Dependent Atmosphere-Ocean Coupled Processes Driving SST Seasonality Changes in a Warmer Climate. *Geophys. Res. Lett.* **51**, e2023GL106953 (2024).
10. Shi, J.-R., Santer, B. D., Kwon, Y.-O. & Wijffels, S. E. The emerging human influence on the seasonal cycle of sea surface temperature. *Nat. Clim. Change* 1–9 (2024) doi:10.1038/s41558-024-01958-8.
11. Weiss, R. F. Carbon dioxide in water and seawater: the solubility of a non-ideal gas. *Mar. Chem.* **2**, 203–

215 (1974).

12. Takahashi, T., Olafsson, J., Goddard, J. G., Chipman, D. W. & Sutherland, S. C. Seasonal variation of CO2 and nutrients in the high-latitude surface oceans: A comparative study. *Glob. Biogeochem. Cycles* **7**, 843–878 (1993).
13. McKinley, G. A., Fay, A. R., Eddebbar, Y. A., Gloege, L. & Lovenduski, N. S. External Forcing Explains Recent Decadal Variability of the Ocean Carbon Sink. *AGU Adv.* **1**, e2019AV000149 (2020).
14. Sarmiento, J. L. & Gruber, N. *Ocean Biogeochemical Dynamics*. (Princeton University Press, 2006).
15. Landschützer, P., Gruber, N., Bakker, D. C. E., Stemmler, I. & Six, K. D. Strengthening seasonal marine CO2 variations due to increasing atmospheric CO2. *Nat. Clim. Change* **8**, 146–150 (2018).
16. Rodgers, K. B. *et al.* Seasonal Variability of the Surface Ocean Carbon Cycle: A Synthesis. *Glob. Biogeochem. Cycles* **37**, e2023GB007798 (2023).
17. Liao, E., Resplandy, L., Liu, J. & Bowman, K. W. Amplification of the Ocean Carbon Sink During El Niños: Role of Poleward Ekman Transport and Influence on Atmospheric CO2. *Glob. Biogeochem. Cycles* **34**, e2020GB006574 (2020).
18. Mignot, A. *et al.* Decrease in air-sea CO2 fluxes caused by persistent marine heatwaves. *Nat. Commun.* **13**, 4300 (2022).
19. Bennington, V., Galjanic, T. & McKinley, G. A. Explicit Physical Knowledge in Machine Learning for Ocean Carbon Flux Reconstruction: The pCO2-Residual Method. *J. Adv. Model. Earth Syst.* **14**, e2021MS002960 (2022).
20. Chau, T.-T.-T., Chevallier, F. & Gehlen, M. Global Analysis of Surface Ocean CO2 Fugacity and Air-Sea Fluxes With Low Latency. *Geophys. Res. Lett.* **51**, e2023GL106670 (2024).
21. Gregor, L., Shutler, J. & Gruber, N. *High Resolution Variability of the Ocean Carbon Sink*. https://essopenarchive.org/users/594276/articles/714620-high-resolution-variability-of-the-ocean-carbon-sink?commit=d7cd490b5dd56270bb8b4f581a153427d9e5480d (2024) doi:10.22541/essoar.170688951.18125151/v1.
22. Landschützer, P., Gruber, N. & Bakker, D. C. E. Decadal variations and trends of the global ocean carbon sink. *Glob. Biogeochem. Cycles* **30**, 1396–1417 (2016).
23. Bakker, D. C. E. *et al.* A multi-decade record of high-quality CO2 data in version 3 of the Surface Ocean CO2 Atlas (SOCAT). *Earth Syst. Sci. Data* **8**, 383–413 (2016).
24. González-Dávila, M., Santana Casiano, J. M. & Machín, F. Changes in the partial pressure of carbon dioxide in the Mauritanian–Cap Vert upwelling region between 2005 and 2012. *Biogeosciences* **14**, 3859–3871 (2017).
25. Bates, N. R., Takahashi, T., Chipman, D. W. & Knap, A. H. Variability of pCO2 on diel to seasonal timescales in the Sargasso Sea near Bermuda. *J. Geophys. Res. Oceans* **103**, 15567–15585 (1998).
26. Sutton, A. J. *et al.* A high-frequency atmospheric and seawater pCO_2 data set from 14 open-ocean sites using a moored autonomous system. *Earth Syst. Sci. Data* **6**, 353–366 (2014).
27. Gürses, Ö. *et al.* Ocean biogeochemistry in the coupled ocean–sea ice–biogeochemistry model FESOM2.1–REcoM3. *Geosci. Model Dev.* **16**, 4883–4936 (2023).
28. Yang, S. & Gruber, N. The anthropogenic perturbation of the marine nitrogen cycle by atmospheric deposition: Nitrogen cycle feedbacks and the 15N Haber-Bosch effect. *Glob. Biogeochem. Cycles* **30**, 1418–1440 (2016).
29. Tsujino, H. *et al.* JRA-55 based surface dataset for driving ocean–sea-ice models (JRA55-do). *Ocean Model.* **130**, 79–139 (2018).
30. Gloege, L. *et al.* Quantifying Errors in Observationally Based Estimates of Ocean Carbon Sink Variability. *Glob. Biogeochem. Cycles* **35**, e2020GB006788 (2021).
31. Hauck, J. *et al.* Sparse observations induce large biases in estimates of the global ocean CO2 sink: an ocean

model subsampling experiment. *Philos. Trans. R. Soc. Math. Phys. Eng. Sci.* **381**, 20220063 (2023).

32. Chatterjee, A. *et al.* Influence of El Niño on atmospheric CO2 over the tropical Pacific Ocean: Findings from NASA's OCO-2 mission. *Science* **358**, eaam5776 (2017).
33. Feely, R. A., Wanninkhof, R., Takahashi, T. & Tans, P. Influence of El Niño on the equatorial Pacific contribution to atmospheric CO2 accumulation. *Nature* **398**, 597–601 (1999).
34. Bunsen, F., Nissen, C. & Hauck, J. The Impact of Recent Climate Change on the Global Ocean Carbon Sink. *Geophys. Res. Lett.* **51**, e2023GL107030 (2024).
35. DeVries, T. *et al.* Magnitude, Trends, and Variability of the Global Ocean Carbon Sink From 1985 to 2018. *Glob. Biogeochem. Cycles* **37**, e2023GB007780 (2023).
36. Müller, J. D. RECCAP2-ocean data collection. Zenodo https://doi.org/10.5281/zenodo.7990823 (2023).
37. Gregor, L., Shutler, J. & Gruber, N. High-Resolution Variability of the Ocean Carbon Sink. *Glob. Biogeochem. Cycles* **38**, e2024GB008127 (2024).
38. Takahashi, T. *et al.* Global sea–air CO2 flux based on climatological surface ocean pCO2, and seasonal biological and temperature effects. *Deep Sea Res. Part II Top. Stud. Oceanogr.* **49**, 1601–1622 (2002).
39. Egleston, E. S., Sabine, C. L. & Morel, F. M. M. Revelle revisited: Buffer factors that quantify the response of ocean chemistry to changes in DIC and alkalinity. *Glob. Biogeochem. Cycles* **24**, n/a-n/a (2010).

Acknowledgments

We acknowledge the contributions from colleagues that helped us to realise this study, including in alphabetical order Nicholas Bates, Thi-Tuyet-Trang Chau, Frédéric Chevallier, Emeric Claudel, Amanda Fay, Melchor González Dávila, Özgür Gürses, Xin Lan, Marguerite Larriere, Damian Loher, J. Magdalena Santana-Casiano, Adrienne Sutton.

JDM and NG acknowledge support from the European Union’s Horizon 2020 research and innovation programme under grant agreements no. 821003 (project 4C) and no. 821001 (SO-CHIC). MG acknowledges funding support by the MOB TAC project of the European Copernicus Marine Environment Monitoring Service (CMEMS) and by the European Union's Horizon Europe Research and innovation program under OceanICU (Grant 101083922). Funding to JH was provided by the Initiative and Networking Fund of the Helmholtz Association (Helmholtz Young Investigator Group MarESys, Grant VH-NG-1301), by the ERC-2022-STG OceanPeak (Grant 101077209) and by the European Union's Horizon Europe research and innovation program under Grant 101083922 (OceanICU). The work reflects only the authors' view; the European Commission and their executive agency are not responsible for any use that may be made. GAM acknowledges support from NSF (LEAP STC AGS2019625, OCE2333608), NOAA (NA20OAR4310340), and ETH Zurich.

517 # Extended data figures and tables

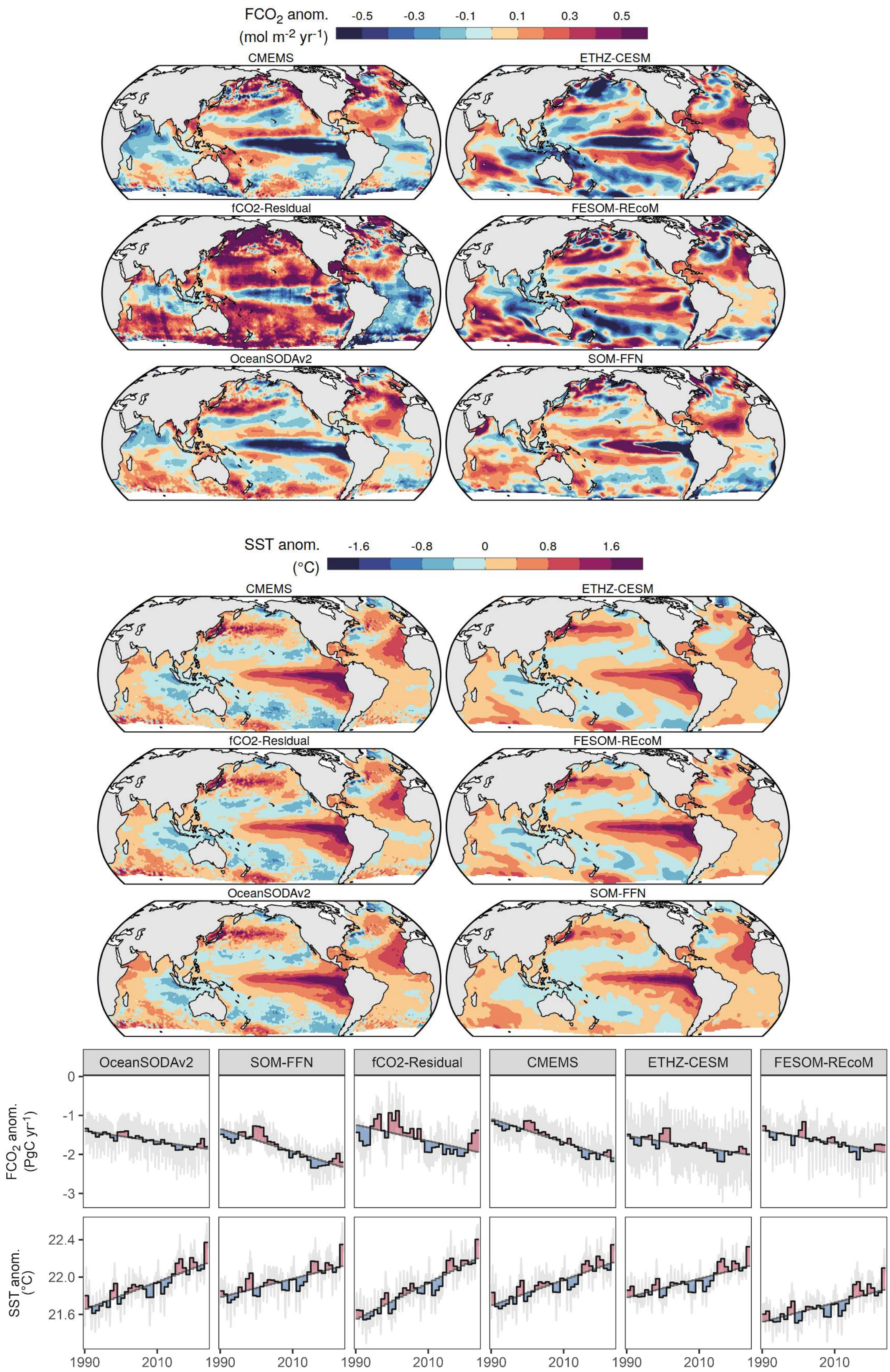

518 **Extended Data Fig. 1**: Same as Fig. 1, but showing the fCO_2 products and GOBMs individually.

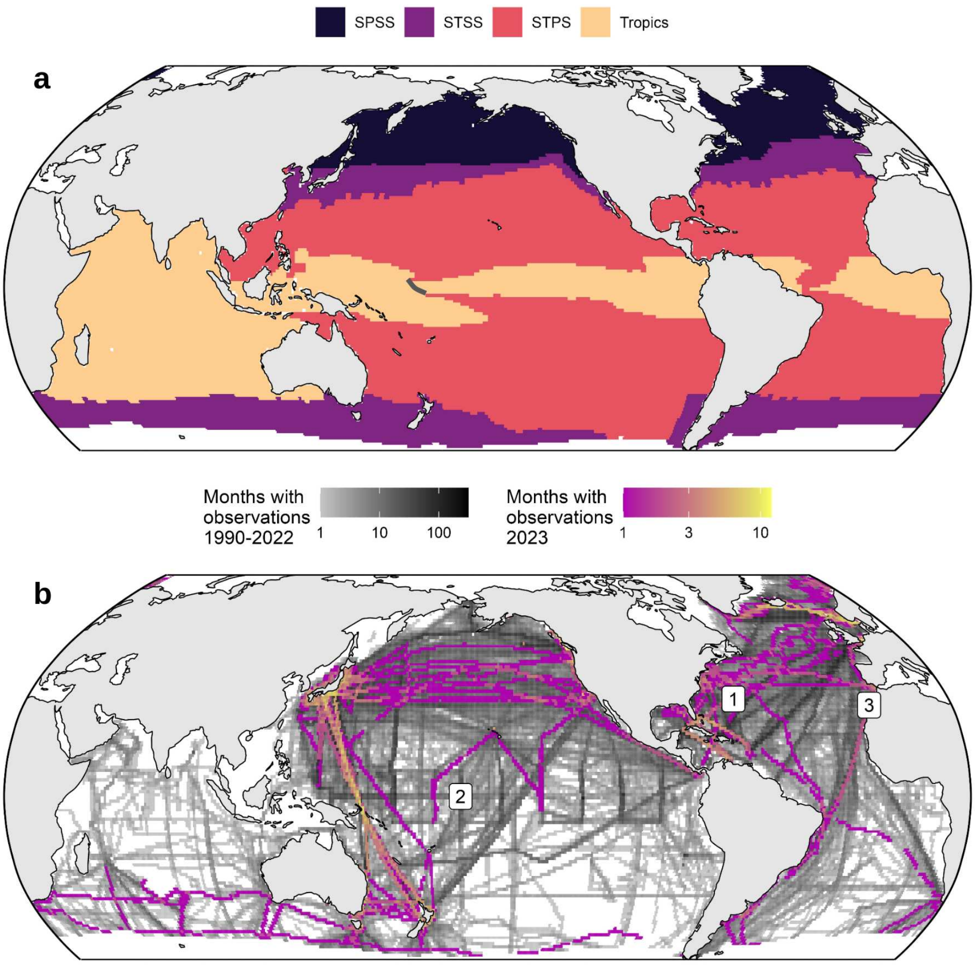

Extended Data Fig. 2: Maps of (a) ocean biomes and (b) fCO_2 observations available from SOCATv2024 for the historical period and 2023. The abbreviations in (a) stand for the subpolar seasonally stratified (SPSS), subtropical seasonally stratified (STSS), subtropical permanently stratified (STPS) biomes. Note that the equatorial Pacific biome is split into an eastern and western part at the black line. These biomes are used to regionally integrate or average spatially resolved estimates. The labels in panel (b) show the three stations for which 2023 observations are compared to the fCO_2 product estimates (see SI): 1 = Bermuda Atlantic Time Series; 2 = Equatorial Pacific; 3 = VOS Line (Gran Canaria - Barcelona).

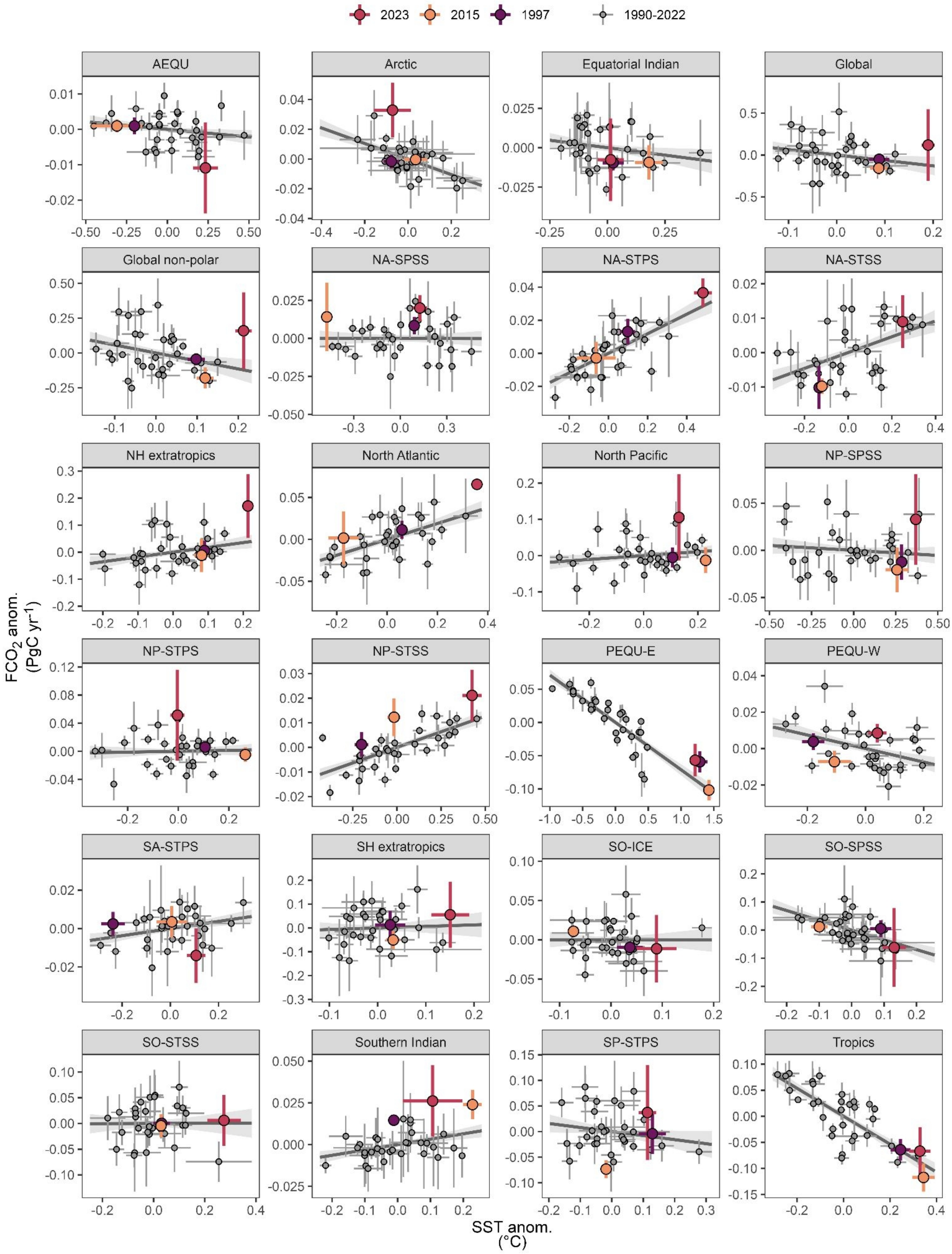

Extended Data Fig. 3: Same as Fig. 2, but showing additional estimates for various biomes and regions as provided also in Table 1.

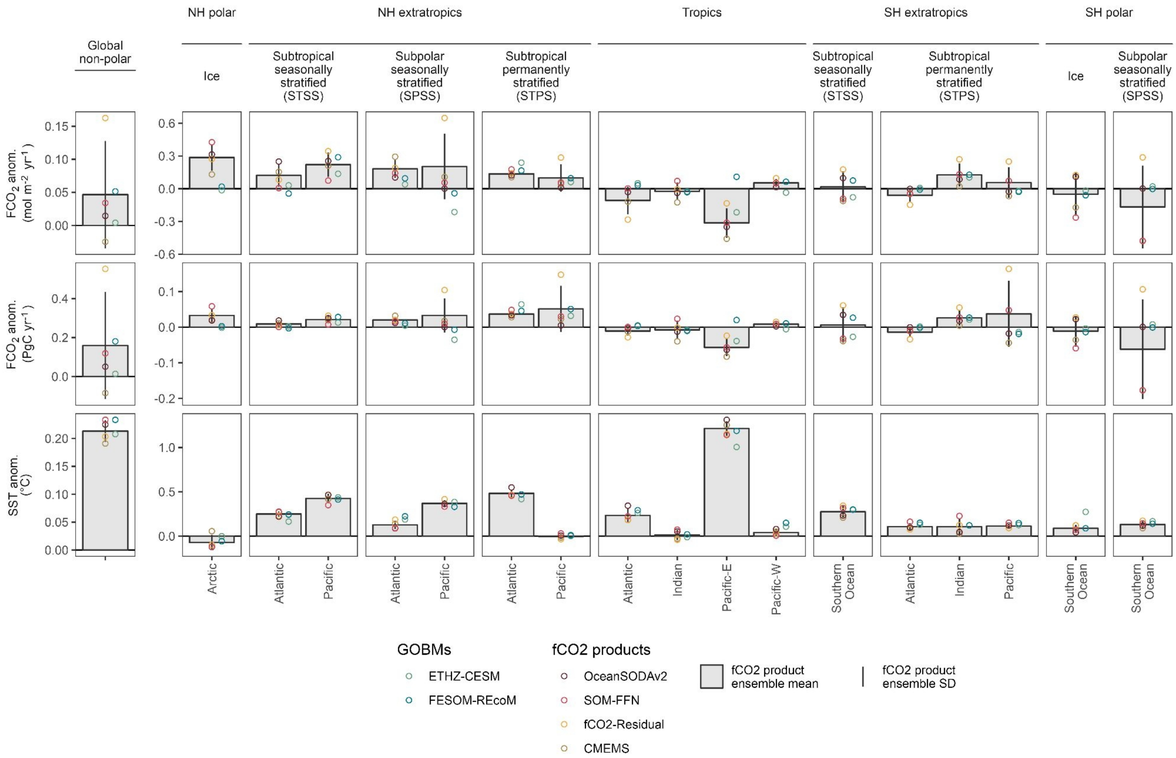

Extended Data Fig. 4: Anomaly estimates from Table 1 displayed as bars (fCO_2 product ensemble mean) with uncertainty ranges (fCO_2 product ensemble standard deviation). In addition, estimates for the individual fCO_2 products and GOBMs are displayed as symbols.

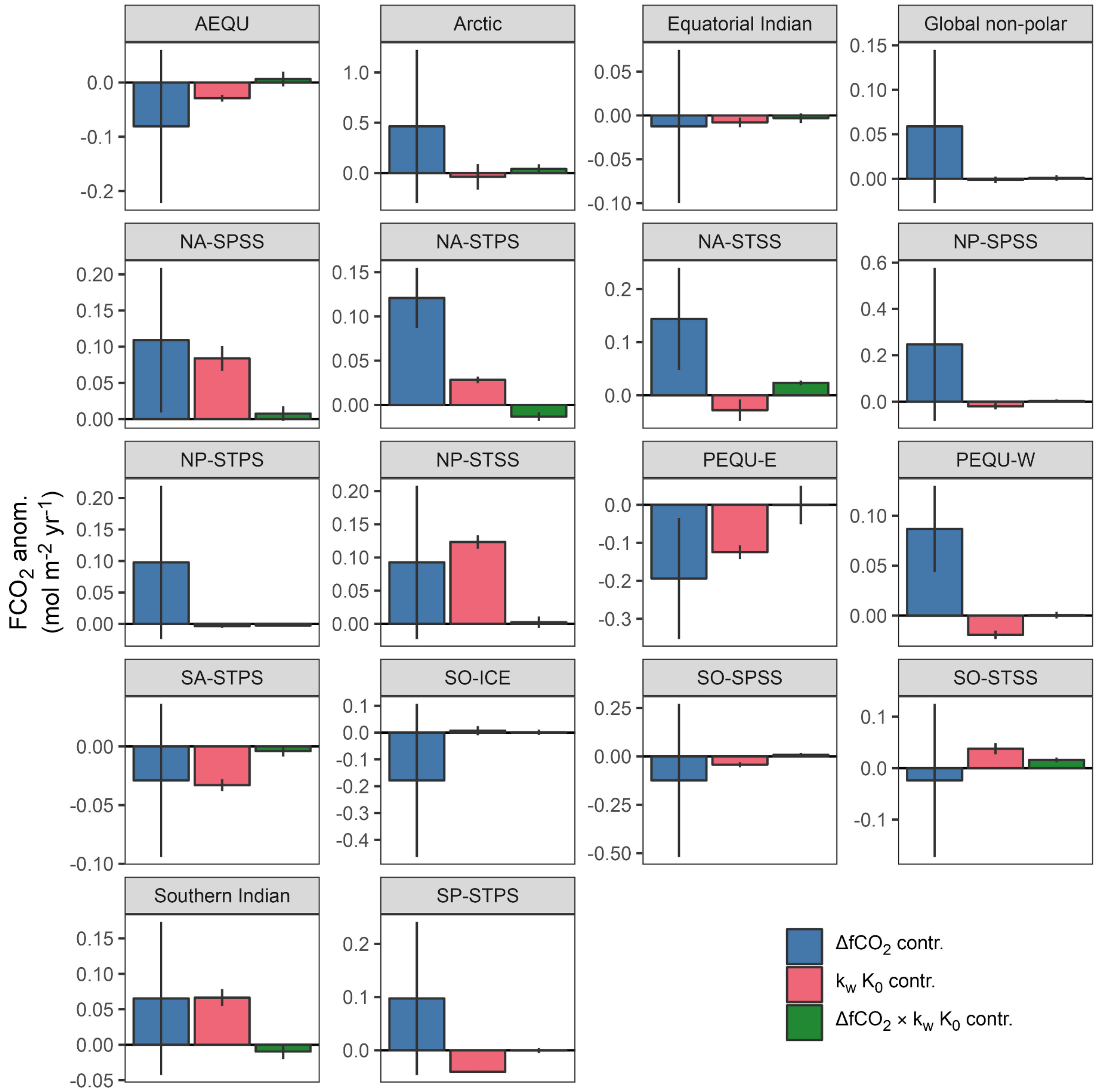

Extended Data Fig. 5: Same estimates as shown in Fig. 3a-c, but averaging the attribution of the 2023 annual mean flux anomalies over the ocean biomes shown in Extended Data Fig. 2. Flux anomalies are attributed to their primary drivers, that is, the CO_2 fugacity gradient between ocean and atmosphere (ΔfCO_2), the product of the gas transfer velocity and the solubility of CO_2 ($k_w K_0$), which is primarily controlled by wind speed, as well as the cross product of both drivers ($\Delta fCO_2 \times k_w K_0$).

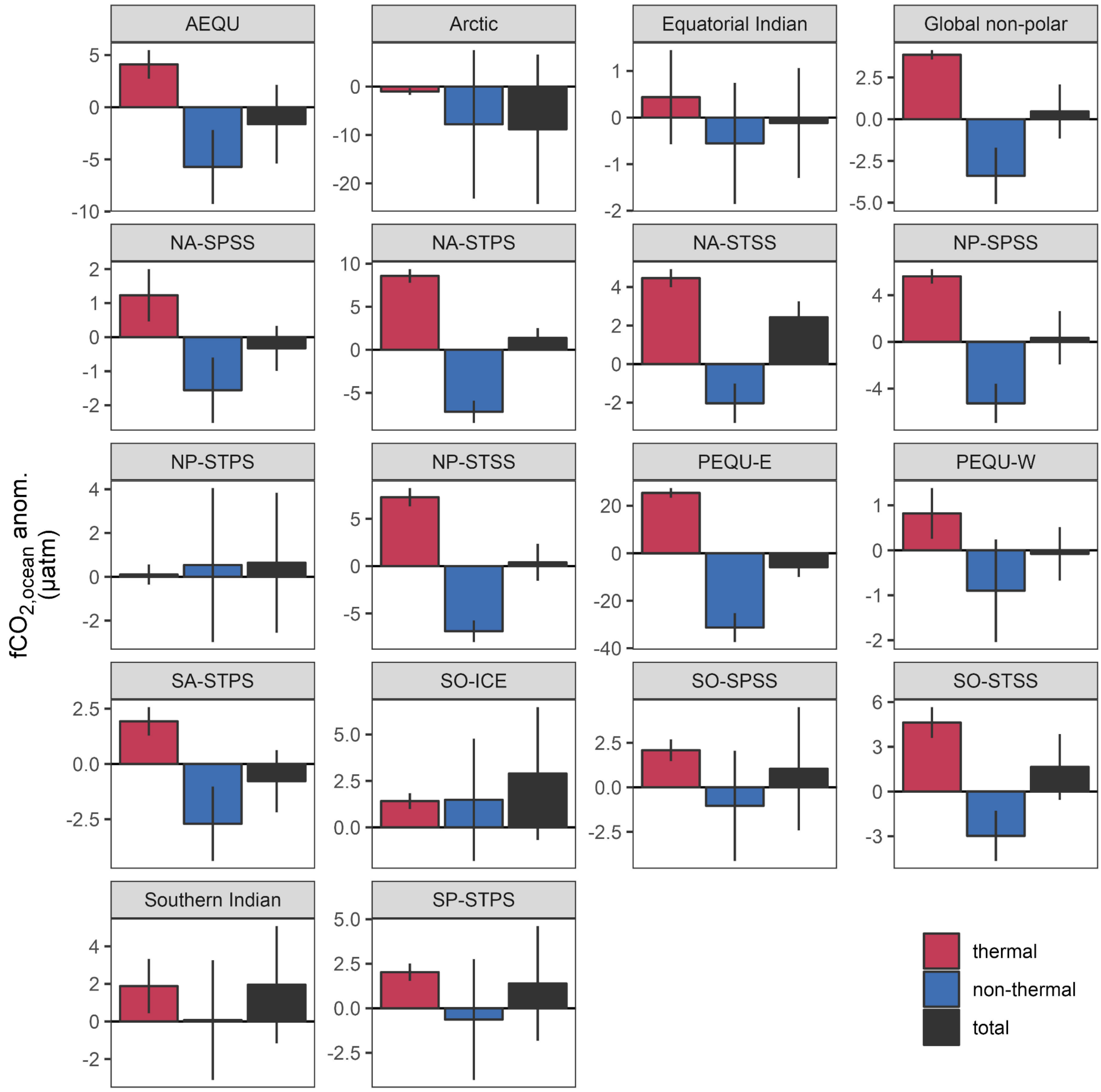

Extended Data Fig. 6: Same estimates as shown in Fig. 3d-f, but averaging the 2023 fCO_2 anomaly decomposition over the ocean biomes shown in Extended Data Fig. 2. Total fCO_2 anomalies (grey) are decomposed into the thermal (red) and non-thermal (blue) components.

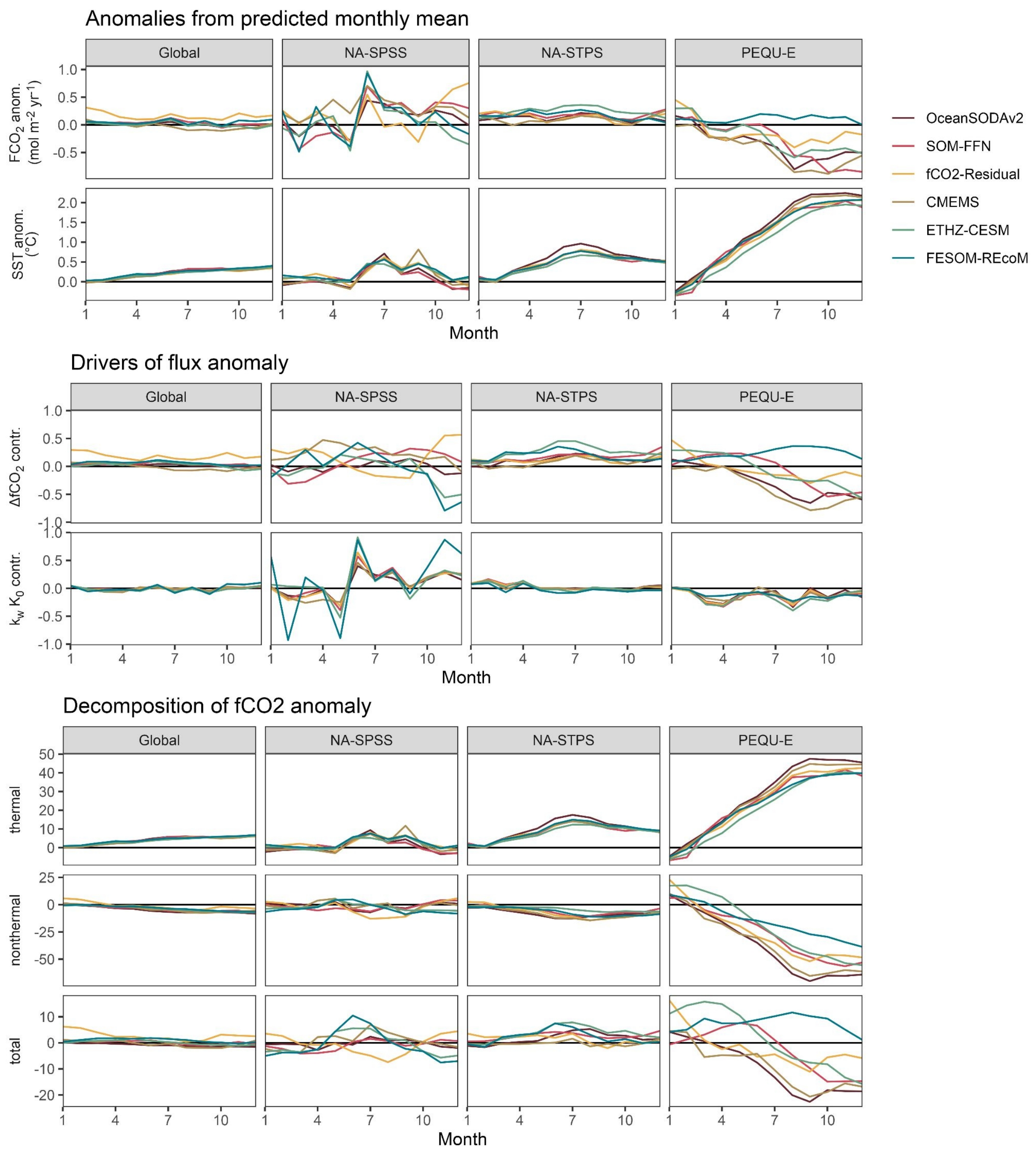

Extended Data Fig. 7: Same as Fig. 3a, but showing the four fCO_2 products and two GOBMs individually. In addition to the three biomes in Fig. 3, estimates for the non-polar global ocean are displayed. Furthermore, the decomposition of the fCO_2 anomalies into their thermal and non-thermal components is shown.

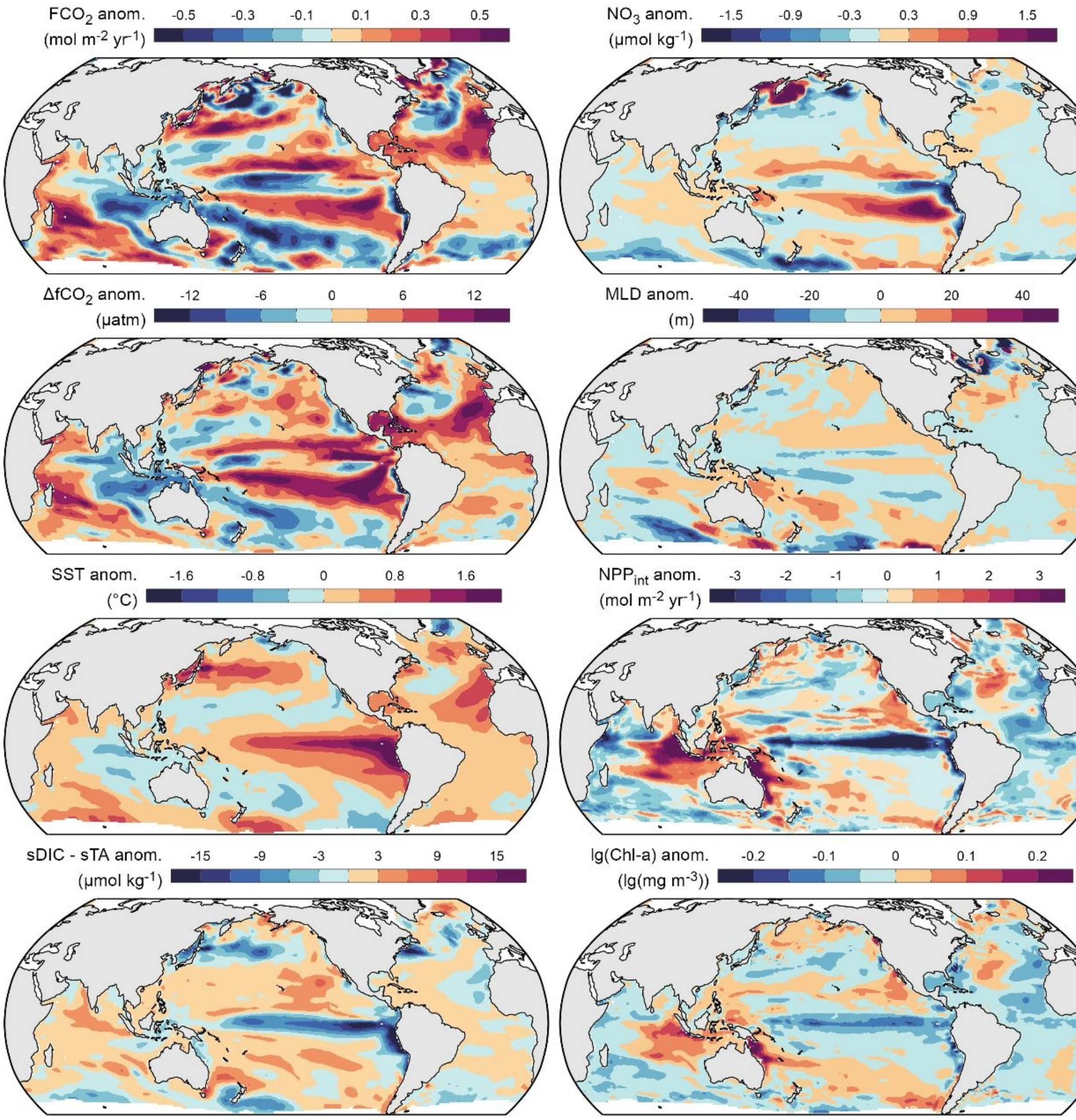

542 **Extended Data Fig. 8**: Annual mean surface anomaly maps based on the mean of two GOBM simulations.

Extended Data Table 1: Details of fCO_2 products. *All fCO_2 products and underlying predictor fields were regridded to a common spatial resolution of 1°x1° and monthly temporal resolution prior to the analysis presented in this study.

Product name	**CMEMS**	**fCO2-Residual**	**SOM-FFN**	**OceanSODAv2**
Reference	Chau et al. (2022)	Bennington et al. (2022)	Landschützer et al. (2016)	Gregor et al. (2024)
Interpolation method	An ensemble of 100 feed-forward neural network models	EXtreme Gradient Boosting (XGB) algorithm applied to fCO_2-Residual (= pCO_2-pCO_2-T). For extension beyond training, $xCO_{2,atm}$ trend is added to reconstructed fCO_2 field.	Clustering-regression approach with self organising map (SOM) and feed-forward neural network (FFN)	Ensemble of clustering-regression approaches
Native resolution*	0.25°x0.25°; monthly	1°x1°; monthly	1°x1°; monthly	0.25°x0.25°; 8-daily
Sea surface fCO_2 training data	SOCATv2023; monthly, 1°x1°	SOCATv2023; monthly, 1°x1°	SOCATv2023; monthly, 1°x1°	SOCATv2023; monthly, 1°x1°
SST predictor	CMEMS	OISST	HadiSST	ESA
SSS predictor	CMEMS	EN4	EN4	SODA/ESA
SSH predictor	CMEMS	-	-	Ssalto/Duacs
Chl-a predictor	CMEMS	Globcolor merged CHL	Globcolor merged CHL	ESA
MLD predictor	ECCO2	deBoyer climatology	Merged MIMOC and deBoyer climatologies	SODA
K_w formulation	Wanninkhof (2014); a adjusted for global mean piston velocity = 16.5 cm/h; scaled by 1-f_{ice}	Wanninkhof (1992) with Schmidt number from Wanninkhof (2014); scaled to bomb 14C (Fay et al., 2021); scaled by 1-f_{ice}	Wanninkhof (1992); a adjusted for global mean piston velocity = 16cm/h; scaled by 1-f_{ice}	Wanninkhof (1992); scaled by 1-f_{ice}
Wind-speed	ERA5	CCMP2, ERA5, JRA55	ERA5	average of ERA5, JRA55, and NCEP1
Atmospheric CO_2	xCO_2 from CAMS inversion; sea level pressure from ERA5; water vapor correction from Weiss (1980)	xCO_2 from NOAA MBL; sea level pressure from ERA5; water vapor correction from Dickson (2007)	xCO_2 from NOAA MBL; sea level pressure from NCEP; water vapor correction from Dickson (2007)	xCO_2 from NOAA MBL; sea level pressure from ERA5; water vapor correction from Dickson (2007)
Sea-ice fraction (f_{ice})	OSTIA/CMEMS product	NOAA OISST	Rayner et al. (2003)	OSTIA

Extended Data Table 2: Details of GOBM simulations. fice is the fractional ice coverage.

Model name	**CESM-ETHZ**	**FESOM-REcoM**
Reference	Doney et al. (2009); Lindsay et al. (2014); Yang and Gruber (2016)	Gürses et al. (2023)
Vertical layers	60	46
Native horizontal resolution	lon: 1.125° lat: 0.27° - 0.53°	1°; refined in equatorial, coastal, and polar regions
Initial conditions	POP2 model using Levitus data and a state of rest, carbonate chemistry from GLODAPv2 pre-industrial	DIC and TA (GLODAPv2 preindustrial); N, Si, and O2 (WOA13); Fe (PISCES, corrected with observations), temperature and salinity from PHC3.0 climatology
Spin up procedure	180 years with CORE forcing and 1850 pCO_2, switch to JRA forcing for 14 years; 3x cycling through JRA with historical forcing	Spun up from 1611-1957 with JRA55-do v1.3, repeating the year 1961.
Length of spin up	180 years (CORE) + 14 years (JRA)	1850-1957
Physical forcing	JRA-55 v1.3	JRA55-do v1.3
K_w parameters	a = 0.31 (Wanninkhof 1992), 1-fice	a = 0.251 (Wanninkhof 2014), 1-fice
Atmospheric CO_2	monthly, global mean xCO_2 (Friedlingstein et al. 2022)	monthly, global mean xCO_2 (Friedlingstein et al. 2022)

Supplementary Files

This is a list of supplementary files associated with this preprint. Click to download.

- MuellerOceanCarbonSink2023SI.pdf